Performance of damaged RC continuous beams strengthened by prestressed laminates plate: Impact of mechanical and thermal properties on interfacial stresses

Hassaine Daouadji Tahar[*1,2], Rabahi Abderezak[1,2], Benferhat Rabia[1,2] and Abdelouahed Tounsi[3,4,5]

[1]*Civil Engineering Department, University of Tiaret, Algeria*
[2]*Laboratory of Geomatics and Sustainable Development, University of Tiaret, Algeria*
[3]*YFL (Yonsei Frontier Lab), Yonsei University, Seoul, Korea*
[4]*LMH Laboratory, Civil Engineering Department, University of Sidi Bel Abbes, Algeria*
[5]*Department of Civil and Environmental Engineering, King Fahd University Saudi Arabia*

Abstract. Strengthening of reinforced concrete beams with externally bonded fiber reinforced polymer plates/sheets technique has become widespread in the last two decades. Although a great deal of research has been conducted on simply supported RC beams, a few studies have been carried out on continuous beams strengthened with FRP composites. This paper presents a simple uniaxial nonlinear analytical model that is able to accurately estimate the load carrying capacity and the behaviour of damaged RC continuous beams flexural strengthened with externally bonded prestressed composite plates on both of the upper and lower fibers, taking into account the thermal load. The model is based on equilibrium and deformations compatibility requirements in and all parts of the strengthened beam, i.e., the damaged concrete beam, the FRP plate and the adhesive layer. The flexural analysis results and analytical predictions for the prestressed composite strengthened damaged RC continuous beams were compared and showed very good agreement in terms of the debonding load, yield load, and ultimate load. The use of composite materials increased the ultimate load capacity compared with the non strengthened beams. The major objective of the current model is to help engineers' model FRP strengthened RC continuous beams in a simple manner. Finally, this research is helpful for the understanding on mechanical behaviour of the interface and design of the FRP-damaged RC hybrid structures.

Keywords: composite plate; interfacial stresses; damaged RC continuous beam; strengthening, shear lag effect

1. Introduction

Strengthening of an existing structure may become necessary because of a required increase in loading capacity and a change in use, as a result of poor design or construction, or as a consequence of deterioration. In such instances, various techniques may be employed to improve the service ability or ultimate performance of the structure (Amara *et al.* 2019, Ashour *et al.* 2004, Panjehpour *et al.* 2016, Smith and Teng 2002, Tounsi 2006, Behnam *et al.* 2020, Al-Furjan *et al.* 2021a,

---

*Corresponding author, Professor, E-mail: daouadjitahar@gmail.com, tahar.daouadji@univ-tiaret.dz

Mansouri *et al*. 2019, Benferhat *et al*. 2021b, Rabahi *et al*. 2021b, Abdelhak *et al*. 2021,Al-Furjan *et al*. 2021b, Al-Furjan *et al*. 2020, Bendada *et al*. 2020, Rabahi *et al*. 2018, Rabia *et al*. 2020, Hassaine Daouadji *et al*. 2008, Khatir *et al*. 2019, Kadir *et al*. 2020, Bendada *et al*. 2020, Bensattalah *et al*. 2018, Benferhat *et al*. 2018, Wang *et al*. 2020). In recent years, the external bonding of carbon or glass FRP plates/sheets to the beam tension face has become a common practice and is widely used to strengthen or repair structures. Strengthening RC beams in flexure with FRP plates/sheets is a powerful strengthening technique due to its simplicity of in situ application, small increase of the beam size and weight, and good resistance to corrosion.

Extensive numerical and experimental research efforts have been carried out to study and model the behavior of simply supported beams with external FRP plates; as a result, there are many design guidelines for such beams (Tounsi 2006, Hassaine Daouadji *et al*. 2016, Smith and Teng 2002). However, many in situ RC beams are used in continuous construction; there has been very limited research into the behavior of such beams with external strengthening. Experimental studies were conducted to compare the behavior of RC continuous beams strengthened with FRP plates with non-strengthened beams (Chaded *et al*. 2018, Guenaneche *et al*. 2014, Akbaş 2020, Mansouri *et al*. 2019, Rabahi *et al*. 2020, Rabia *et al*. 2016, Roumaissa *et al*. 2020, Hassaine Daouadji *et al*. 2019, Liu *et al*. 2019, Mohammed Sakr *et al*. 2016, Pello *et al*. 2020, Rabahi *et al*. 2019, Alimirzaei *et al*. 2019, Benhenni *et al*. 2019, Bensattalah *et al*. 2020, Benferhat *et al*. 2019, Rabahi *et al*. 2021a, Hassaine Daouadji *et al*. 2021, Bekki *et al*. 2021, Benferhat *et al*. 2021a, Guellil *et al*. 2021, Rabia *et al*. 2019, Bensatallah *et al*. 2020, Tlidji *et al*. 2021, Kablia *et al*. 2020, Hassaine Daouadji 2017, Chikr *et al*. 2020, Hassaine Daouadji 2013, Hamrat *et al*. 2020, Bekki *et al*. 2019, Chergui *et al*. 2019, Benferhat *et al*. 2020, Benhenni *et al*. 2018, Xue-jun *et al*. 2019, Cheng *et al*. 2019, Hassaine Daouadji *et al*. 2020). They concluded that the use of FRP plates/sheets to strengthen continuous beams was effective for reducing deflections and for increasing their load carrying capacity. The problem of interfacial stresses when prestressed laminates are used in strengthening and repair has treated only by Rabahi (2016) and Benachour *et al*. (2008). In investigation, the interfacial shear and normal stress was studied, a rigorous solution for interfacial stresses in simply supported beams strengthened with bonded prestressed FRP plate is developed, however, did not consider the effects of bending and thermal deformation in the plate and shear deformations model in the beam. In this paper, a new theoretical solution and a general model are developed to predict both shear and normal interfacial stress with bonded prestressed FRP laminates and an improved new shear lag and prestressed laminates model are developed for a damaged reinforced concrete continuous beam bonded with a prestressed composite, this beam is subject to a thermo mechanical loading coupled q (uniformly distributed load); P_0 (prestressing force of composite plate) and ΔT (Thermal load).

The research work presented in this paper develops a new nonlinear model that is able to simulate the mechanical behavior of FRP-strengthened RC continuous beams utilizing realistic nonlinear constitutive relations for each strengthened beam component. The interfacial shear and normal stresses in the adhesive layer are presented using an analytical model based on nonlinear fracture mechanics. This model introduces accurate predictions for the ultimate load of FRP-strengthened RC continuous beams and; a sound mechanical description and interpretation for failure modes. With this in mind, the objectives of this paper are first to present an improvement to existing solutions in the literature to obtain a new closed-form solution which accounts for the parabolic adherend shear deformation effect in both the beam and bonded plate and second to compare quantitatively its solution against the new one developed in this paper by numerical illustrations. Numerical examples and a parametric study are presented to illustrate the governing parameters that control the stress concentrations at the edge of the FRP strip. Finally, the adopted improved model
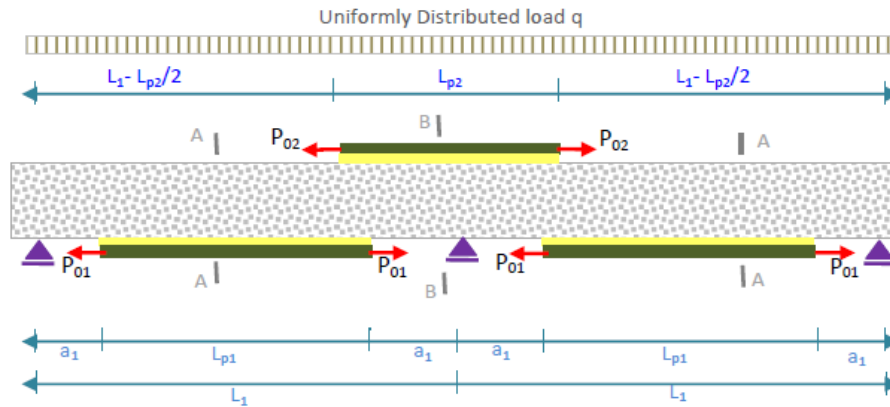
Fig. 1 Damaged reinforced concrete continuous beam bonded with a prestressed composite plate

describes better the actual response of the damaged reinforced concrete continuous beam bonded with a prestressed composite and permits the evaluation of the adhesive stresses, the knowledge of which is very important in the design of such structures. It is believed that the present results will be of interest to civil and structural engineers and researchers.

2. Research significance

The most common failure modes for FRP-strengthened RC beams are debonding of the FRP plate or ripping of the concrete cover. These types of failures prevent the strengthened beam for reaching its ultimate flexural capacity, and therefore they must be included in design considerations. In order to avoid premature ruptures, a closed form solution of stress concentrations must be presented, taking into account in this analysis several parameters influencing the behavior of the hybrid concrete-composite structure, such as:
    - Geometry of the beam, this time it is a continuous reinforced concrete beam,
    - Effect of damage to the concrete of the beam,
    - Effect of air bubbles (defect in manufacturing concrete; in other words, the porosity of concrete),
    - Effect of prestressing composite materials,
    - Coupled loading: Thermo mechanical load "a Uniformly distributed load (q), a Prestressing load (P_0) coupled with a Thermal load ($\alpha\Delta T$)".

3. Method of solution

3.1 Assumptions of the present solution

Fig. 1 shows the geometry of the damaged RC continuous beam reinforced with prestressed composite plate, and the configuration of the interface of the adhesive layer and the applied load are shown in Fig. 2. The terms V, M, and N present, respectively, the shear force, the bending moment, and the longitudinal tension, while the continuous beam and the FRP plate are symbolized,
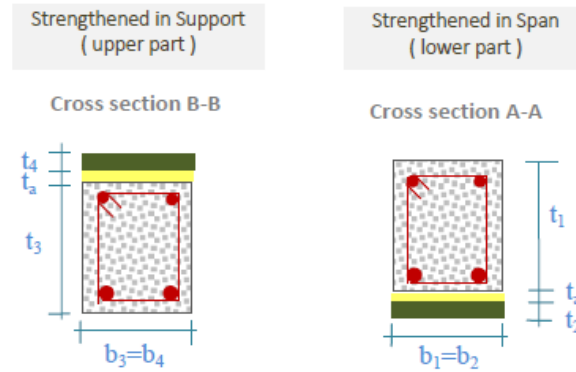
Fig. 2 Continuous damaged reinforced concrete beam bonded with a prestressed composite plate: cross section in span and cross in support

respectively, by 1 and 2, $\tau(x)$ and $\sigma_n(x)$ are the shear stress and normal stress, and "t" is the component thickness. This analytical and numerical model is madding by the following assumptions:

The analytical approach (Hassaine Daouadji *et al*. 2016) is based on the following assumptions:
- Elastic stress strain relationship for composite material plate and adhesive;
- There is a perfect bond between the composite material plate and the continuous beam;
- The adhesive is assumed to only play a role in transferring the stresses from the damaged RC continuous beam to the prestressed composite plate reinforcement;
- The stresses in the adhesive layer do not change through the direction of the thickness.

3.2 Material properties of damaged concrete beams

The model's Mazars is based on elasticity coupled with isotropic damage and ignores any manifestation of plasticity, as well as the closing of cracks (Mazars *et al*. 1996). This concept directly describes the loss of rigidity and the softening behavior. The stresses is determined by the following expression

$$\sigma_{ij} = (1-\varphi)E_{ij}\varepsilon_{ij} = \widehat{E}_{ij}\varepsilon_{ij} \qquad 0 < d < 1 \tag{1}$$

$$\widehat{E}_{11} = E_{11}(1-\varphi) \text{ long} \tag{2}$$

$$\widehat{E}_{22} = E_{22}(1-\varphi) \text{ trans} \tag{3}$$

where $\widehat{E}_{11}$, $\widehat{E}_{22}$ and E_{11}, E_{22} are the elastic constants of damaged and undamaged state, respectively. "φ" is damaged variable. Hence, the material properties of the damaged beam can be represented by replacing the above elastic constants with the effective ones defined in Eqs. (2) and (3).

3.3 Distribution forms of the air bubbles in the concrete beam

Because of manufacturing defects in concrete such as the air bubbles "α" that are the subject of the subject, the Young's modulus (E_1) of the imperfect reinforced concrete beam can be written as a functions of thickness coordinate. Several forms of porosity (air bubbles in concrete) have been
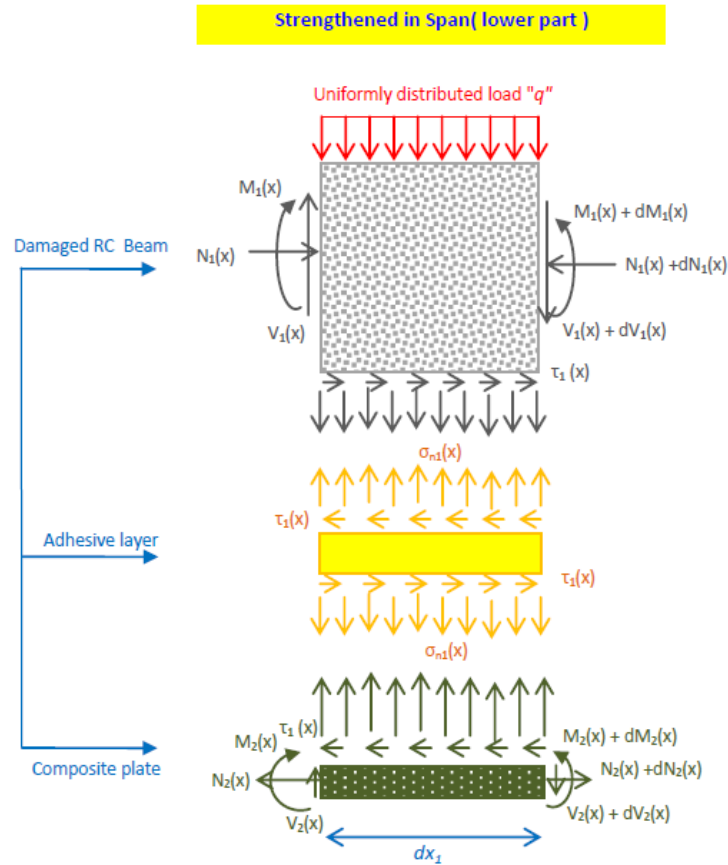
Fig. 3 Forces in infinitesimal element of a continuous damaged reinforced concrete beam bonded with a prestressed composite plate in span "lower part"

studied in the present work, which is written in the following forms

$$\breve{E}_1 = E_b(1 - \mu) \tag{4}$$

$$\sigma_{ij} = (1 - \mu)E_{ij}\varepsilon_{ij} = \breve{E}_{ij}\varepsilon_{ij} \tag{5}$$

where $\breve{E}_1$ and E_b is the elastic constants of imperfect and perfect state concrete and μ is the index of air bubbles in concrete.

3.4 Mathematical formulation of the present method "Strengthened in span: lower part"

A differential section *dx*, can be cutout from the composite- strengthened damaged RC continuous beam, as shown in Fig. 3 "Strengthened in Span: lower part". The strains in the damaged RC continuous beam near the adhesive interface and the external FRP reinforcement can be expressed in this method.

3.4.1 Interfacial shear stresses "Strengthened in span: lower part"

The deformation in concrete in the vicinity of the adhesive layer can be expressed by

$$\varepsilon_1(x) = \frac{du_1(x)}{dx} = \frac{y_1}{\tilde{E}_1 I_1} M_1(x) + \frac{N_1(x)}{\tilde{E}_1 A_1} + \frac{t_1}{4G_1} \frac{d\tau(x)}{dx} + \alpha_1 \Delta T \tag{6}$$

Based on the theory of laminated sheets, the deformation of the composite sheet in the vicinity of the adhesive layer is given by

$$\varepsilon_2(x) = \frac{du_2(x)}{dx} = -\frac{y_2}{E_2 I_2} M_2(x) + \frac{P_{01} + N_2(x)}{E_2 A_2} + \frac{5t_2}{12G_2} \frac{d\tau(x)}{dx} + \alpha_2 \Delta T \tag{7}$$

Where $u_1(x)$ and $u_2(x)$ are the horizontal displacements of the concrete beam and the composite plate respectively. $M_1(x)$ and $M_2(x)$ are respectively the bending moments applied to the concrete beam and the composite plate; P_{01} is the compression force in the beam due to prestressing, $\tilde{E}_1$ is the Young's modulus of concrete with the taking into account the state of damage and the effect of air bubbles; I_1 the moment of inertia, N_1 and N_2 are the axial forces applied to the concrete and the composite plate respectively, b_2 and t_2 are the width and thickness of the reinforcement plate, ΔT is the temperature change.

In what follows, the stiffness of the reinforcement plate is significantly lower than that of the concrete beam to be reinforced. The bending moment in the composite plate can be neglected to simplify the shear stress derivation operations.

The shear stress at the adhesive layer can be expressed as follows

$$\tau_a = \tau(x) = K_s \Delta u(x) = K_s \left[u_2(x) - u_1(x) \right] \tag{8}$$

Where K_s is the shear stiffness of the adhesive layer per unit length. From Eq. (8) we can deduce the expression of K_s which is given by

$$K_s = \frac{\tau(x)}{\Delta u(x)} = \frac{\tau(x)}{\Delta u(x)/t_a} \frac{1}{t_a} = \frac{G_a}{t_a} \tag{9}$$

$\Delta u(x)$ is the displacement relative to the adhesive interface, G_a et t_a are the modulus and thickness of the adhesive layer, respectively.

By differentiating the Eqs. (8), (6) and (7) with respect to x, and neglecting the bending moment of the composite plate we will have

$$\frac{d\tau(x)}{dx} = \frac{G_a}{t_a} \left[(-D_{11}' \frac{y_2}{b_2} M_2(x) + A_{11}' \frac{P_{01} + N_2(x)}{b_2} + \alpha_2 \Delta T) - (\frac{y_1}{\tilde{E}_1 I_1} M_1(x) + \frac{N_1}{\tilde{E}_1 A_1} + \alpha_1 \Delta T) \right] \tag{10}$$

By differentiating Eq. (10) we will have

$$\frac{d^2\tau(x)}{dx^2} = K_s \left[(\frac{A_1}{b_2} \frac{dN_2(x)}{dx} - A_2 \frac{t_2}{2b_2} \frac{dM_2(x)}{dx} + \alpha_2 \Delta T) - (\frac{y_1}{E_1 I_1} \frac{dM_1(x)}{dx} + \frac{1}{E_1 A_1} \frac{dN_1(x)}{dx} + \alpha_1 \Delta T) \right]$$
$$- K_s (\frac{5t_2}{12G_2} + \frac{1}{4G_1}) \frac{d^2\tau(x)}{dx^2} \tag{11}$$

Substituting $\frac{dM_1(x)}{dx}$, $\frac{dM_2(x)}{dx}$ and $N(x)$ with their following expressions in Eq. (11)

$$N_1(x) = -N(x) = -N_2(x) = -b_2 \int_0^x \tau(x) \qquad (12)$$

$$\frac{dM_1(x)}{dx} = \frac{R_{1-2}}{R_{1-2}+1} \left[V_{T1-2}(x) - b_2\tau(x)(y_1 + t_a + \frac{t_2}{2}) \right] \qquad (13)$$

$$\frac{dM_2(x)}{dx} = \frac{1}{R_{1-2}+1} \left[V_{T1-2}(x) - b_2\tau(x)(y_1 + t_a + \frac{t_2}{2}) \right] \qquad (14)$$

Allows us to obtain the differential equation of the shear interface stress

$$\frac{d^2\tau(x)}{dx^2} - K_1 b_2 \left[\frac{(y_1+y_2)(y_1+y_2+t_a)}{\widetilde{E}_1 I_1 + E_2 I_2} + \frac{1}{\widetilde{E}_1 A_1} + \frac{1}{E_2 A_2} \right]\tau(x) + K_1 \left[\frac{y_1+y_2}{\widetilde{E}_1 I_1 + E_2 I_2} \right] V_{T_{1-2}}(x) = 0 \quad (15)$$

Where

$$K_1 = \frac{1}{\dfrac{t_a}{G_a} + \dfrac{t_1}{4G_1} + \dfrac{5t_2}{12G_2}} \qquad (16)$$

For simplicity, the general solutions presented below are limited to loading which is either concentrated or uniformly distributed over part or the whole span of the beam, or both. For such loading, $d^2V_T(x)/dx^2=0$, and the general solution to Eq. (15) is given by

$$\tau(x) = \eta_1 \cosh(\xi x) + \eta_2 \sinh(\xi x) + \frac{K_1}{\xi^2} \left[\frac{(y_1+y_2)}{\widetilde{E}_1 I_1 + E_2 I_2} \right] V_{T1-2}(x) \qquad (17)$$

Where

$$\xi = \sqrt{K_1 b_2 \left[\frac{(y_1+y_2)(y_1+y_2+t_a)}{\widetilde{E}_1 I_1 + E_2 I_2} + \frac{1}{\widetilde{E}_1 A_1} + \frac{1}{E_2 A_2} \right]} \qquad (18)$$

And η_1 and η_2 are constant coefficients determined from the boundary conditions. In the present study, a simply supported beam has been investigated which is subjected to a uniformly distributed load.

For our case of a uniformly distributed load, the formula of the shear stress is given by the following equation

$$\tau(x) = \left[\frac{1}{\xi}(\frac{t_a}{G_a} + \frac{t_1}{4G_1})(\frac{A_{11}'}{b_2}P_{01} - \frac{y_1 M_{t1-2}(0)}{\widetilde{E}_1 I_1} + (\alpha_2 + \alpha_1)\Delta T) \right] e^{-\xi x}$$

$$+ (a_1 q + x - \frac{e^{-\xi x}}{\xi}q)\frac{K_1}{\xi^2} \left[\frac{(y_1+y_2)}{\widetilde{E}_1 I_1 + E_2 I_2} \right] \qquad 0 \le x \le L_{P1} \qquad (19)$$

3.4.2 Interfacial normal stresses "Strengthened in span: lower part"

The following governing differential equation for the interfacial normal stress (Hassaine Daouadji *et al*. 2016)

$$\frac{d^4\sigma_n(x)}{dx^4} + \frac{E_a b_2}{t_a}(\frac{1}{\widetilde{E}_1 I_1} + \frac{1}{E_2 I_2})\sigma_n(x) + \frac{E_a b_2}{t_a}(\frac{y_1}{\widetilde{E}_1 I_1} - \frac{y_2}{E_2 I_2})\frac{d\tau(x)}{dx} + \frac{q E_a}{t_a \widetilde{E}_1 I_1} = 0 \quad (20)$$

The general solution to this fourth-order differential equation is

$$\sigma_n(x) = e^{-\rho x}[\eta_3 \cos(\rho x) + \eta_3 \sin(\rho x)] + e^{\rho x}[\eta_5 \cos(\rho x) + \eta_6 \sin(\rho x)] - n_1\frac{d\tau(x)}{dx} - n_2 q \quad (21)$$

For large values of x it is assumed that the normal stress approaches zero and, as a result, $\eta_5 = \eta_6 = 0$. The general solution therefore becomes

$$\sigma_n(x) = e^{-\rho x}[\eta_3 \cos(\rho x) + \eta_4 \sin(\rho x)] - \frac{y_1 E_2 I_2 - y_2 \widetilde{E}_1 I_1}{\widetilde{E}_1 I_1 + E_2 I_2}\frac{d\tau(x)}{dx} - \frac{E_2 I_2}{b_2(\widetilde{E}_1 I_1 + E_2 I_2)}q \quad (22)$$

Where

$$\rho = \sqrt[4]{\frac{E_a b_2}{4 t_a}(\frac{1}{\widetilde{E}_1 I_1} + \frac{1}{E_2 I_2})} \quad (23)$$

$$n_1 = \frac{y_1 E_2 I_2 - y_2 \widetilde{E}_1 I_1}{\widetilde{E}_1 I_1 + E_2 I_2} \quad (24)$$

and

$$n_2 = \frac{E_2 I_2}{b_2(\widetilde{E}_1 I_1 + E_2 I_2)} \quad (25)$$

As is described by Tounsi (2006), the constants η_3 and η_4 in Eq. (22) are determined using the appropriate boundary conditions and they are written as follows

$$\eta_3 = \frac{E_a[V_{T1-2}(0) + \rho M_{T1-2}(0)]}{2\rho^2 \widetilde{E}_1 I_1} - \frac{E_a}{t_a 2\rho^3}(\frac{y_1 b_2}{E_1 I_1} - \frac{y_2 b_2}{E_2 I_2})\tau(0) + \\ + \frac{y_1 E_2 I_2 - y_2 \widetilde{E}_1 I_1}{2\rho^3(\widetilde{E}_1 I_1 + E_2 I_2)}(\frac{d^4\tau(0)}{dx^4} + \rho\frac{d^3\tau(0)}{dx^3}) \quad (26)$$

$$\eta_4 = \frac{-E_a M_{T1-2}(0)}{2\rho^2 t_a \widetilde{E}_1 I_1} - \frac{y_1 E_2 I_2 - y_2 \widetilde{E}_1 I_1}{2\rho^2(\widetilde{E}_1 I_1 + E_2 I_2)}\frac{d^3\tau(0)}{dx^3} \quad (27)$$

The above expressions for the constants ϕ_3 and ϕ_4 has been left in terms of the bending moment $M_{T1-2}(0)$ and shear force $V_{T1-2}(0)$ at the end of the soffit plate. With the constants η_3 and η_4 determined, the interfacial normal stress can then be found using Eq. (22).

3.5 Mathematical formulation of the present method "Strengthened in support: Upper part"

A differential section dx, can be cutout from the composite- strengthened damaged RC continuous beam, as shown in Fig. 4 "Strengthened in Support: upper part". The strains in the damaged RC continuous beam near the adhesive interface and the external FRP reinforcement can be expressed in this theory.
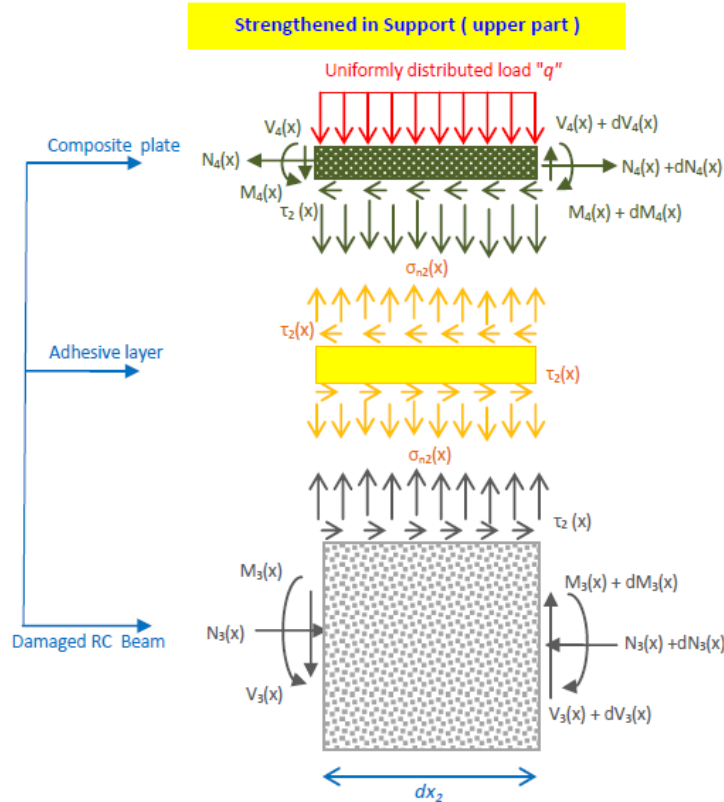
Fig. 4 Forces in infinitesimal element of a continuous reinforced concrete beam bonded with a prestressed composite plate in support "upper part"

3.5.1 Adhesive shear stress distribution along the FRP-concrete interface "Strengthened in support: Upper part"

The deformation in concrete in the vicinity of the adhesive layer can be expressed by

$$\varepsilon_3(x) = \frac{du_3(x)}{dx} = \frac{y_3}{\tilde{E}_3 I_3} M_3(x) + \frac{N_3(x)}{\tilde{E}_3 A_3} + \frac{t_3}{4G_3} \frac{d\tau_a}{dx} + \alpha_3 \Delta T \qquad (28)$$

Based on the theory of laminated sheets, the deformation of the prestressed laminate composite sheet in the vicinity of the adhesive layer is given by

$$\varepsilon_4(x) = \frac{du_4(x)}{dx} = -D_{11}' \frac{t_4}{2b_4} M(x) + A_{11}' \frac{P_{02} + N_4(x)}{b_4} + \alpha_4 \Delta T \qquad (29)$$

Where $u_3(x)$ and $u_4(x)$ are the horizontal displacements of the concrete beam and the composite plate respectively. $M_3(x)$ and $M_4(x)$ are respectively the bending moments applied to the concrete beam and the composite plate; P_{02} is the compression force in the beam due to prestressing, $\tilde{E}_3$ is the Young's modulus of concrete with the taking into account the state of damage and the effect of air bubbles; I_3 the moment of inertia, N_3 and N_4 are the axial forces applied to the concrete and the composite plate respectively, b_4 and t_4 are the width and thickness of the reinforcement plate, ΔT the

temperature difference, $[A']=[A^{-1}]$ is the inverse of the membrane matrix $[A]$, $[D']=[D^{-1}]$ is the inverse of the bending matrix.

In what follows, the stiffness of the reinforcement plate is significantly lower than that of the concrete beam to be reinforced. The bending moment in the composite plate can be neglected to simplify the shear stress derivation operations.

The shear stress at the adhesive layer can be expressed as follows

$$\tau_a = \tau(x) = K_s \Delta u(x) = K_s \left[u_4(x) - u_3(x) \right] \tag{30}$$

Where K_s is the shear stiffness of the adhesive layer per unit length. From equation (30) we can deduce the expression of K_s which is given by

$$K_s = \frac{\tau(x)}{\Delta u(x)} = \frac{\tau(x)}{\Delta u(x)/t_a} \frac{1}{t_a} = \frac{G_a}{t_a} \tag{31}$$

$\Delta u(x)$ is the displacement relative to the adhesive interface, G_a et t_a are the modulus and thickness of the adhesive layer, respectively.

By differentiating the Eqs. (30), (28) and (29) with respect to x, and neglecting the bending moment of the composite plate we will have

$$\frac{d\tau(x)}{dx} = K_s \left[\left[-D_{11}' \frac{y_4}{b_4} M_4(x) + A_{11}' \frac{P_{02} + N_4(x)}{b_4} + \alpha_4 \Delta T \right] - \left[\frac{y_3}{\widetilde{E}_3 I_3} M_3(x) + \frac{N_3}{\widetilde{E}_3 A_3} + \frac{t_3}{4G_3} + \alpha_3 \Delta T \right] \right] \tag{32}$$

By differentiating Eq. (32) we will have

$$\frac{d^2\tau(x)}{dx^2} = \frac{4G_3 G_a}{4G_3 t_a + G_a t_3} \left[\left(\frac{A_{11}'}{b_4} \frac{dN_4(x)}{dx} - D_{11}' \frac{t_4}{2b_4} \frac{dM_4(x)}{dx} + \alpha_4 \Delta T \right) - \left(\frac{y_3}{\widetilde{E}_3 I_3} \frac{dM_3(x)}{dx} + \frac{1}{\widetilde{E}_3 A_3} \frac{dN_3(x)}{dx} + \alpha_3 \Delta T \right) \right]$$
$$- K_s \left(\frac{5t_4}{12G_4} + \frac{1}{4G_3} \right) \frac{d^2\tau(x)}{dx^2} \tag{33}$$

Substituting $\frac{dM_3(x)}{dx}$, $\frac{dM_4(x)}{dx}$ and $N(x)$ with their following expressions in Eq. (33)

$$N(x) = N_4(x) = N_3(x) = b_4 \int_0^x \tau(x) \tag{34}$$

$$\frac{dM_3(x)}{dx} = \frac{R_{3-4}}{R_{3-4}+1} \left[V_{T3-4}(x) - b_4 \tau(x)(y_3 + t_a + \frac{t_4}{2}) \right] \tag{35a}$$

$$\frac{dM_4(x)}{dx} = \frac{1}{R_{3-4}+1} \left[V_{T3-4}(x) - b_4 \tau(x)(y_3 + t_a + \frac{t_4}{2}) \right] \tag{35b}$$

Allows us to obtain the differential equation of the shear interface stress

$$\frac{d^2\tau(x)}{dx^2} - \frac{4G_3 G_a}{4G_3 t_a + G_a t_3} \left[A_{11}' + \frac{b_4}{\widetilde{E}_3 A_3} + \frac{(2y_3 + t_4)(2y_3 + 2t_a + t_4)}{4(\widetilde{E}_3 I_3 D_{11}' + b_4)} b_4 D_{11}' \right] \tau(x)$$
$$+ \left[\frac{4G_3 G_a}{4G_3 t_a + G_a t_3} \left(\frac{(2y_3 + t_4)}{2(\widetilde{E}_3 I_3 D_{11}' + b_4)} D_{11}' \right) \right] V_T(x) = 0 \tag{36}$$

The solution to the differential equation (Eq. (36)) above is given by

$$\tau(x) = \eta_7 \cosh(\delta x) + \eta_8 \sinh(\delta x) + m_1 V_{T3-4}(x) \tag{37}$$

$$\tau(x) = \eta_7 \cosh(\delta x) + \eta_8 \sinh(\delta x) + \frac{4G_3 G_a}{\delta^2 (4G_3 t_a + G_a t_3)} \left(\frac{(2y_3 + t_4)}{2(\tilde{E}_3 I_3 D_{11}' + b_4)} D_{11}' \right) V_{T3-4}(x) \tag{38}$$

With

$$\delta = \sqrt{\frac{4G_3 G_a}{4G_3 t_a + G_a t_3} \left[A_{11}' + \frac{b_4}{\tilde{E}_3 A_3} + \frac{(2y_3 + t_4)(2y_3 + 2t_a + t_4)}{4(\tilde{E}_3 I_1 D_{11}' + b_4)} b_4 D_{11}' \right]} \tag{39}$$

$$m_1 = \frac{1}{2\delta^2} \left(\frac{t_a}{G_a} + \frac{t_3}{4G_3} \right) \left(\frac{(2y_3 + t_4)}{\tilde{E}_3 I_3 D_{11}' + b_4} D_{11}' \right) \tag{40}$$

And η_7 and η_8 are constant coefficients determined from the boundary conditions. In the present study, a simply supported beam has been investigated which is subjected to a uniformly distributed load.

For our case of a uniformly distributed load, the formula of the shear stress is given by the following equation

$$\tau(x) = \eta_8 e^{-\delta x} + m_1 q(a + x) \qquad\qquad 0 \leq x \leq L_{P2} \tag{41}$$

With

$$\eta_8 = \frac{1}{\delta} \left(\frac{t_a}{G_a} + \frac{t_1}{4G_3} \right) \left(\frac{A_{11}'}{b_4} P_{02} - \frac{y_3 M_{t3-4}(0)}{\tilde{E}_3 I_3} + (\alpha_4 - \alpha_3)\Delta T \right) - \frac{m_1 q}{\delta} \tag{42}$$

3.5.2 Adhesive normal stress distribution along the FRP-concrete interface "Strengthened in support: Upper part"

The following governing differential equation for the interfacial normal stress (Hassaine Daouadji *et al.* 2016)

$$\frac{d^4 \sigma_n(x)}{dx^4} + \frac{E_a}{t_a} \left(D_{11}' + \frac{b_4}{\tilde{E}_3 I_3} \right) \sigma_n(x) - K_n \left(D_{11}' \frac{t_4}{2} - \frac{y_3 b_4}{\tilde{E}_3 I_3} \right) \frac{d\tau(x)}{dx} + \frac{q E_a}{\tilde{E}_3 I_3 t_a} = 0 \tag{43}$$

The general solution of the differential equation of order 4 is

$$\sigma_n(x) = e^{-\lambda x} \left[\eta_9 \cos(\lambda x) + \eta_{10} \sin(\lambda x) \right] + e^{\lambda x} \left[\eta_{11} \cos(\lambda x) + \eta_{12} \sin(\lambda x) \right] -$$
$$- \left(\frac{2y_3 b_4 - D_{11}' \tilde{E}_3 I_3 t_4}{2(D_{11}' \tilde{E}_3 I_3 + b_4)} \right) \frac{d\tau(x)}{dx} - \frac{q}{D_{11}' \tilde{E}_3 I_3 + b_4} \tag{44}$$

For large values of "x" we assume that the normal stress tends to zero, and it results $\eta_{11} = \eta_{12} = 0$. The general solution becomes

$$\sigma_n(x) = e^{-\lambda x} \left[\eta_9 \cos(\lambda x) + \eta_{10} \sin(\lambda x) \right] - \frac{2y_3 b_4 - D_{11}' \tilde{E}_3 I_3 t_4}{2(D_{11}' \tilde{E}_3 I_3 + b_4)} \frac{d\tau(x)}{dx} - \frac{q_2}{D_{11}' \tilde{E}_3 I_3 + b_4} \tag{45}$$

Where:

$$\lambda = \sqrt[4]{\frac{E_a}{4t_a}(D_{11}^{'} + \frac{b_4}{\tilde{E}_3 I_3})}$$ (46)

The integration constants η_9 and η_{10} are given by

$$\eta_9 = \frac{E_a}{2\lambda^3 t_a \tilde{E}_3 I_3}[V_{T3-4}(O) + \lambda M_{T3-4}(O)] - \frac{b_4 E_a}{2\lambda^3 t_a}(\frac{y_3}{\tilde{E}_3 I_3} - \frac{D_{11}^{'} t_4}{2b_4})\tau(O) +$$ (47)
$$+ (\frac{2 y_3 b_4 - D_{11}^{'}\tilde{E}_3 I_3 t_4}{4\lambda^3 (D_{11}^{'}\tilde{E}_3 I_3 + b_4)})(\frac{d^4 \tau(O)}{dx^4} + \lambda \frac{d^3 \tau(O)}{dx^3})$$

$$\eta_{10} = -\frac{E_a}{2\lambda^2 t_a \tilde{E}_3 I_3} M_{T3-4}(O) - \frac{2 y_3 b_4 - D_{11}^{'}\tilde{E}_3 I_3 t_4}{4\lambda^2 (D_{11}^{'}\tilde{E}_3 I_3 + b_4)} \frac{d^3 \tau(O)}{dx^3}$$ (48)

4. Numerical results and discussions

4.1 Geometric and material properties

The material used for the present studies is an RC damaged continuous beam bonded with a glass, carbon and borone fiber reinforced plastic (GFRP, CFRP and BFRP) plate.

The RC damaged continuous beam is subjected to a uniformly distributed load. A summary of the geometric and material properties is given in Table 1 and Fig. 5. The span of the RC damaged continuous beam is (L_{p1}=2600 mm, L_{p2}=2000 mm), the distance from the support to the end of the plate is 200 mm and the uniformly distributed load (UDL) is 50 kN/ml.

4.2 Comparison with analytical solutions

The analytical model of the structural components has been employed to validate the results of the above procedure. The geometry of the reinforced beam is shown in Fig. 5. In this case, numerical results are presented to study the effect of the linear taper model on the distribution of interfacial stresses in RC damaged continuous beam strengthening with prestressed laminate plate. Figs. 6 and 7 shows the plots of the interfacial stresses for the coupled thermo mechanical loading ($q; P_0$ and ΔT). The present prediction of the interfacial edge stresses is compared with that developed by

Table 1 Geometric and mechanical properties of the materials used

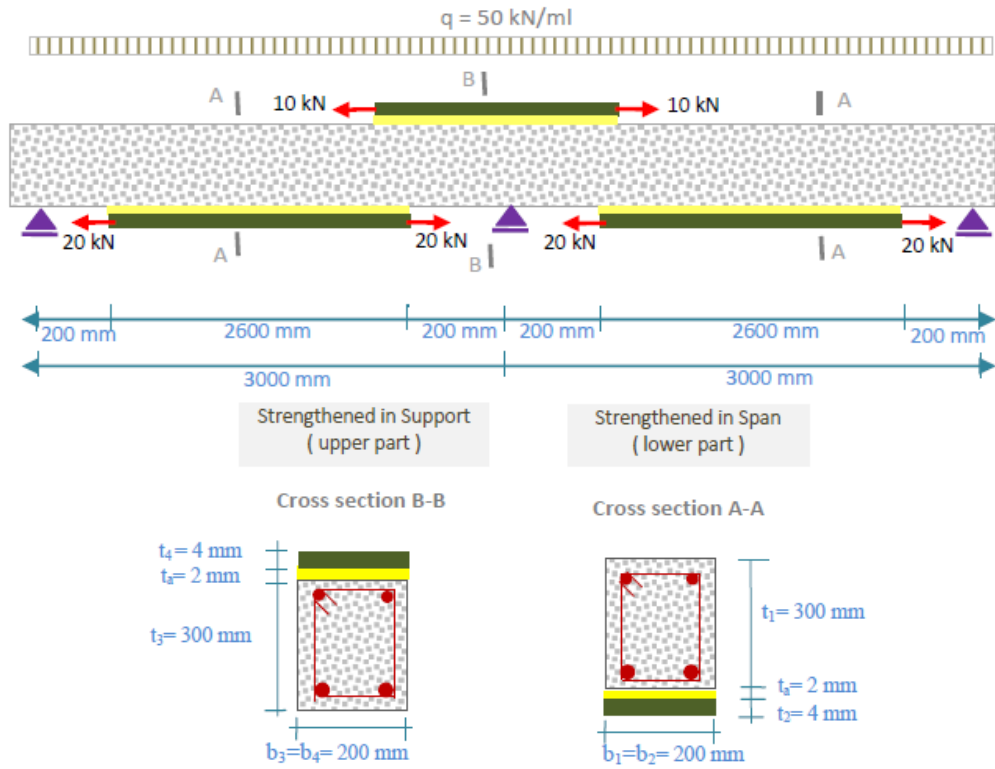| Component	Width (mm)	Depth (mm)	Young's modulus (MPa)	Poisson's ratio
RC beam	b_1=200	t_1=300	E_1=30000	0.18
Adhesive layer	b_1=100	t_a=2	E_a=6700	0.4
Borone fiber	b_1=100	t_2=4	E_2=410 000	0.3
HR Carbon fiber	b_1=100	t_2=4	E_2=140 000	0.28
E Glass fiber	b_1=100	t_2=4	E_2=73 000	0.22
Matrix	--	--	E_m=3520	0.34

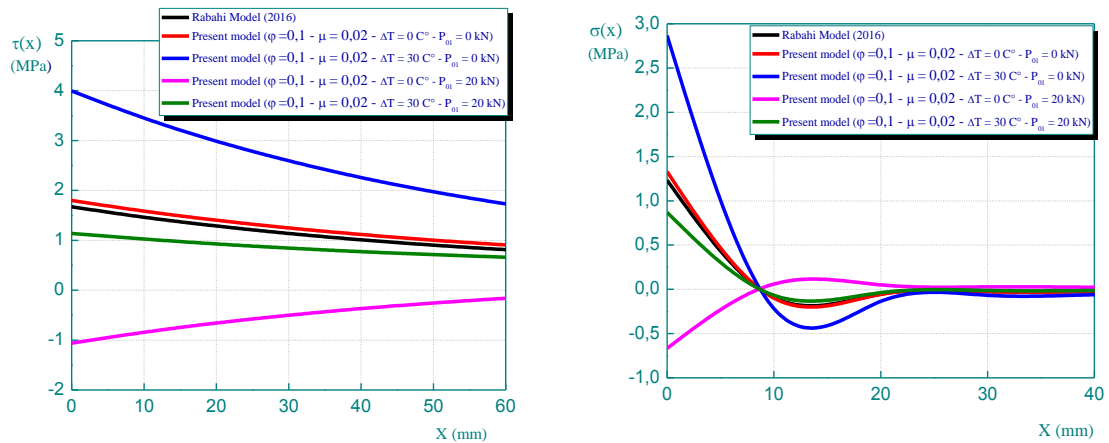Fig. 5 Geometric characteristic of a RC damaged continuous beam bonded with a prestressed composite plate

Fig. 6 Variations of interfacial stresses in RC damaged continuous beam strengthening with prestressed laminate plate: Comparison between the analytical model "Strengthened in span: Lower part"

Rabahi (2016) for an applied thermal load (ΔT= 30°C) an uniformly distributed load (q=50 kN/ml) and a prestressing force (P_{01}=20 kN and P_{01}=10 kN), Figs. 6 and 7 show an almost exact agreement between results. Consequently, The interface stress distributions obtained by the present study and other existing models are shown in good agreement. As demonstrated, good agreements of the
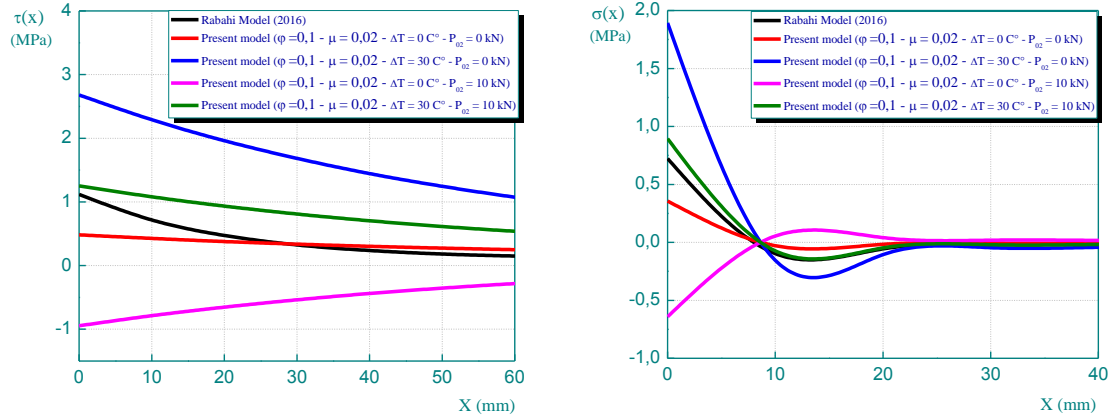
Fig. 7 Variations of interfacial stresses in RC damaged continuous beam strengthening with prestressed laminate plate: Comparison between the analytical model "Strengthened in support: Upper part"
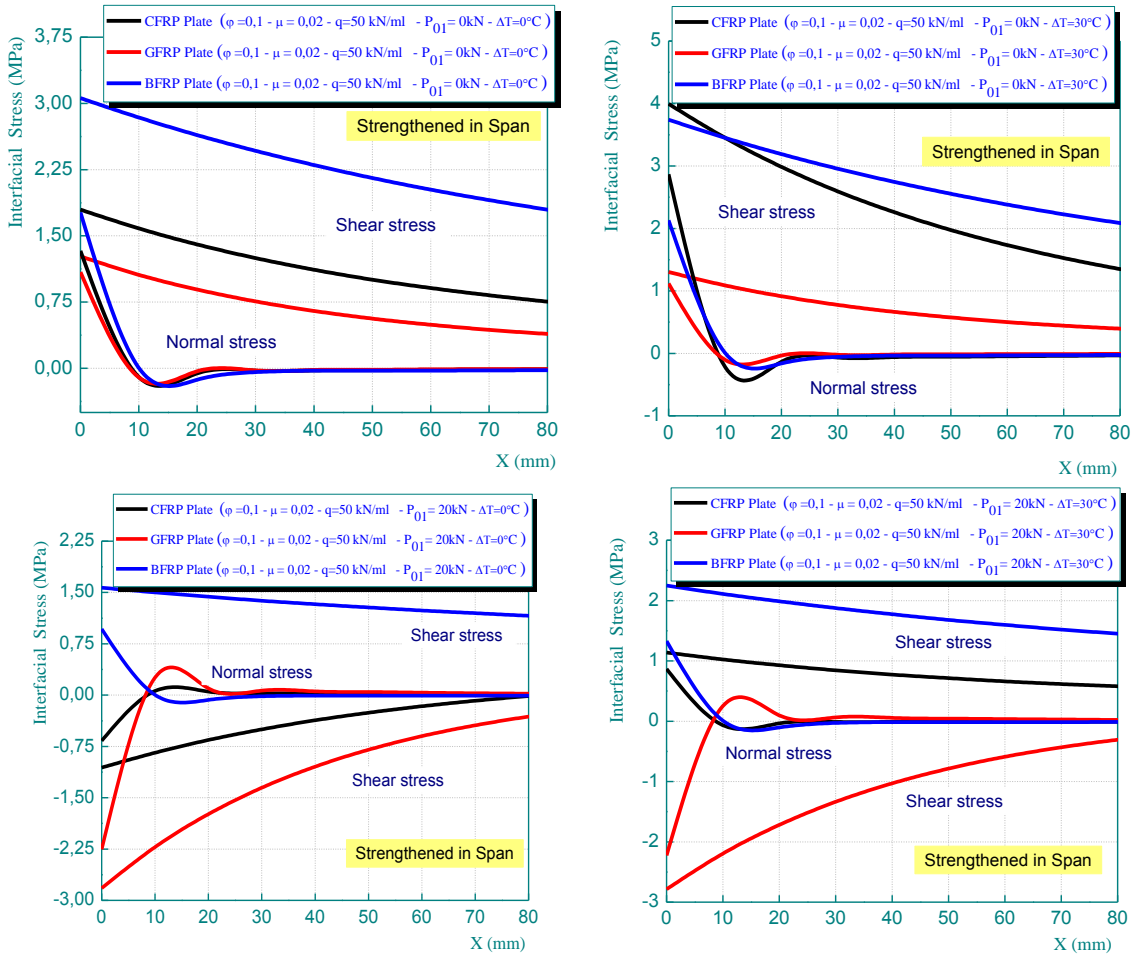

Fig. 8 Effect of the rigidity of composite plate on interfacial stresses for a continuous RC damaged beam Strengthened with presstresed composite plate: Strengthened in span
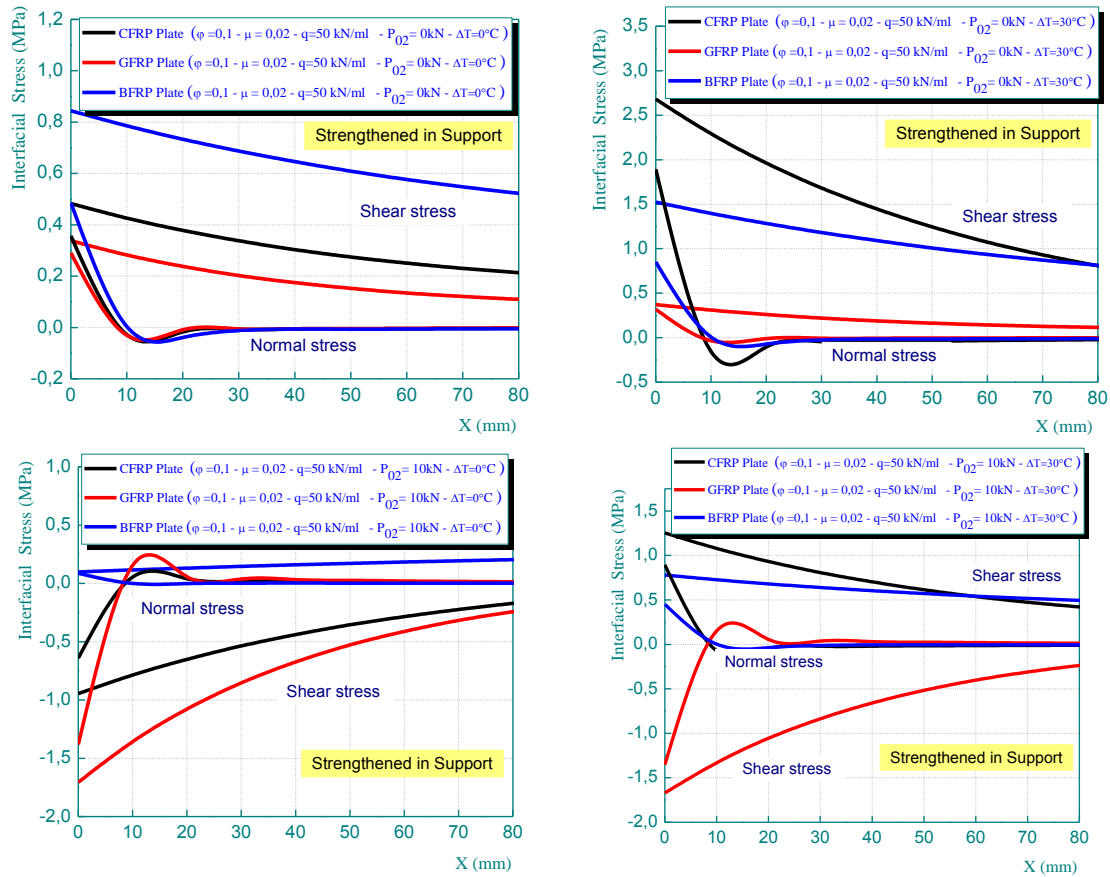
Fig. 9 Effect of the rigidity of composite plate on interfacial stresses for a continuous RC damaged beam strengthened with presstresed composite plate: Strengthened in support

interfacial stresses among all the comparisons are reached at the plate end. The concentrations decay fast along the adhesive layer and reduce to the composite beam solution at a sufficient distance away from the plate end.

4.3 Interfacial stresses for different parameters

After verifying the accuracy of the present analytical model, a parameter study is carried out to better understand the effects of various parameters on the interfacial stresses under the coupling of different applied load (q; P_0 and ΔT).

4.3.1 Effect of plate stiffness on interfacial stress

Figs. 8 and 9 gives interfacial normal and shear stresses for the RC beam bonded with a CFRP plate, GFRP plate and BFRP plate, respectively, which demonstrates the effect of plate material properties on interfacial stresses. The length of the plate is $Lp1$=2600 mm and $Lp1$=2000 mm, and the thickness of the plate and the adhesive layer are both 4 mm. The RC damaged continuous beam strengthening with prestressed laminate and submitted under different types of loading by combining
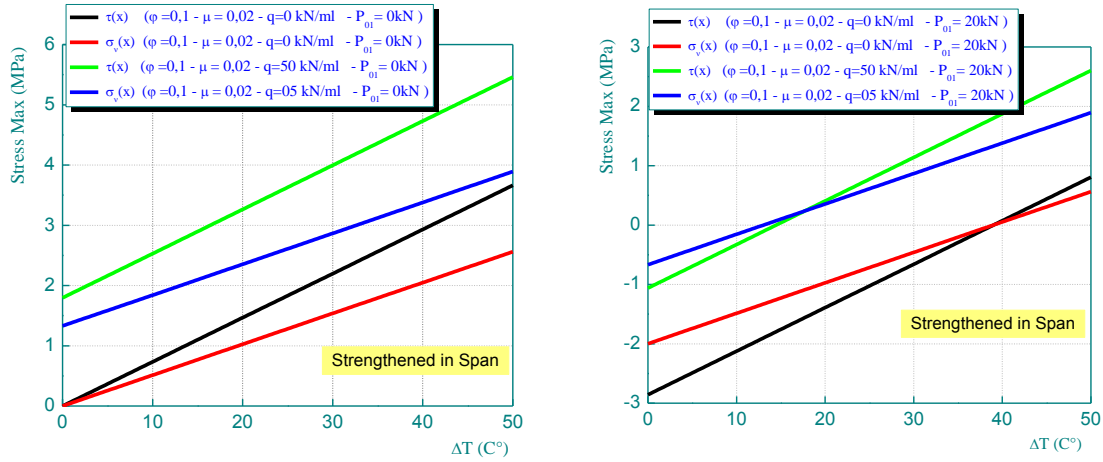
Fig. 10 Effect of temperature variation on interfacial stresses for a continuous RC damaged beam strengthened with presstresed composite plate: Strengthened in span
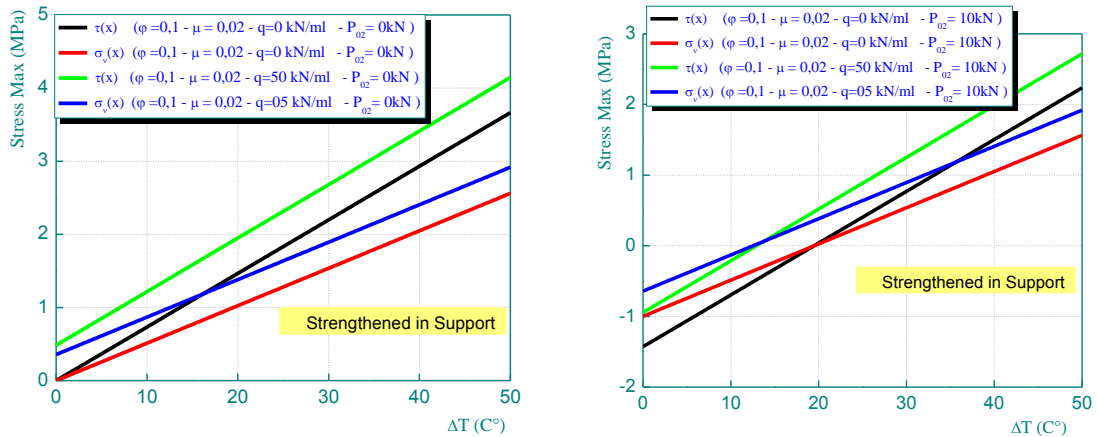

Fig. 11 Effect of temperature variation on interfacial stresses for a continuous RC damaged beam strengthened with presstresed composite plate: Strengthened in support

between the parameters of loads (q; P_0 and ΔT) and the effect of the porosity and the damage of the concrete. The results show that, as the plate material becomes softer (from BFRP to CFRP and then GFRP), the interfacial stresses become smaller, as expected. This is because, under the same load, the tensile force developed in the plate is smaller, which leads to reduced interfacial stresses. The position of the peak interfacial shear stress moves closer to the free edge as the plate becomes less stiff.

4.3.2 Effect of temperature variation

The effect of the thermal load on the distribution of interfacial stresses at the end of the laminate is illustrated in Fig. 10 and 11, and we notice that the higher values of shear and normal stresses correspond with the higher values of relative the temperature. Table 2 presents the maximum values of interfacial stresses for the different values of temperature (0°C, 10°C, 20°C, 30°C, 40°C and

50°C).

4.3.3 Effect of the concrete damage variable

Table 3 show the effect of damage extent on maximum shear and normal interfacial stresses, respectively, for the CFRP materials. Taking into account the parameters influencing the behavior of the reinforced beam; such as: the porosity of the concrete with a thermo mechanical loading coupled q (uniformly distributed load); P_0 (prestressing force of composite plate) and ΔT (Thermal load). The results show that when the damage variable φ increases from 0 to 0.3, the maximum interfacial stress increases slowly.

4.3.4 Effect of variation of the prestressing force of composite plate

Effect of the prestressing force (P_{01} and P_{02}) on adhesive stress: In this section, numerical results of the present solution are presented to study the effect of the prestressing force P_{01} and P_{02} on the distribution of interfacial stress in a RC damaged continuous beam strengthened with bonded prestressed FRP plate. Twice Seven values of P0 are considered in this study, namely: a series in span P_{01}=0 kN; P_{01}=10 kN; P_{01}=20 kN; P_{01}=30 kN; P_{01}=40 kN; P_{01}=50 kN and a series in support P_{02}=0 kN; P_{02}=1 kN; P_{02}=2 kN; P_{02}=3 kN; P_{02}=4 kN; P_{02}=5 kN, while taking into account the porosity of the concrete and the damage effect of the concrete beam. Table 4 and Fig. 12 plot the

Table 2 Effect of temperature variation on interfacial stresses for a continuous RC damaged beam strengthened with presstresed composite plate

Effect of temperature variation on interfacial stresses for a continuous RC damaged beam strengthened with presstresed composite plate							
Case of the strengthened in span with Index of porosity μ=0,02 and Damage variable φ=0,1							
Load	ΔT (C°)	0°C	10°C	20°C	30°C	40°C	50°C
q=00 kN/ml	$\tau(x)$ (MPa)	0,00000	0,73268	1,46537	2,19805	2,93074	3,66342
P_{01}=0 kN	$\sigma_n(x)$ (MPa)	0,00000	0,51221	1,02441	1,53662	2,04882	2,56102
q=50 kN/ml	$\tau(x)$ (MPa)	1,79764	2,53032	3,26301	3,99569	4,72838	5,46106
P_{01}=0 kN	$\sigma_n(x)$ (MPa)	1,32960	1,84180	2,35401	2,86622	3,37842	3,89062
q=00 kN/ml	$\tau(x)$ (MPa)	-2,85733	-2,12465	-1,39196	-0,65928	0,07341	0,80609
P_{01}=20 kN	$\sigma_n(x)$ (MPa)	-1,99751	-1,48530	-0,97310	-0,46089	0,05131	0,56351
q=50 kN/ml	$\tau(x)$ (MPa)	-1,05968	-0,32700	0,40569	1,13837	1,87106	2,60374
P_{01}=20 kN	$\sigma_n(x)$ (MPa)	-0,66791	-0,15571	0,35650	0,86871	1,38091	1,89311
Case of the strengthened in support with Index of porosity μ=0,02 and Damage variable φ=0,1							
q=00 kN/ml	$\tau(x)$ (MPa)	0,00000	0,73268	1,46537	2,19805	2,93073	3,66342
P_{01}=0 kN	$\sigma_n(x)$ (MPa)	0,00000	0,51221	1,02441	1,53662	2,04882	2,56102
q=50 kN/ml	$\tau(x)$ (MPa)	0,48302	1,21570	1,94839	2,68107	3,41375	4,14644
P_{01}=0 kN	$\sigma_n(x)$ (MPa)	0,35719	0,86939	1,38160	1,89381	2,40601	2,91821
q=00 kN/ml	$\tau(x)$ (MPa)	-1,42866	-0,69598	0,03671	0,76939	1,50207	2,23476
P_{01}=10 kN	$\sigma_n(x)$ (MPa)	-0,99876	-0,48655	0,02565	0,53786	1,05006	1,56226
q=50 kN/ml	$\tau(x)$ (MPa)	-0,94565	-0,21297	0,51972	1,25240	1,98508	2,71777
P_{01}=10 kN	$\sigma_n(x)$ (MPa)	-0,64157	-0,12936	0,38284	0,89505	1,40725	1,91945

Table 3 Effect of the concrete damage variable on interfacial stresses for a continuous RC damaged beam strengthened with presstresed composite plate

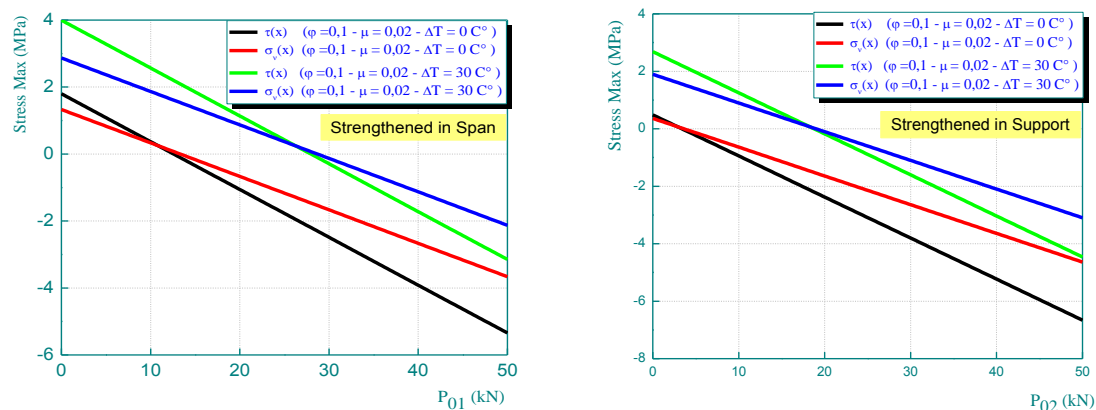| Effect of the concrete damage variable on interfacial stresses for a continuous RC damaged beam strengthened with presstresed composite plate					
Case of the strengthened in span with Index of porosity μ=0,02					
Load	Damage variable	φ=0	φ=0,1	φ=0,2	φ=0,3
q=50 kN/ml ΔT=0°C P_{01}=0 kN	$\tau(x)$ (MPa)	1,69220	1,79764	1,92119	2,06849
	$\sigma_n(x)$ (MPa)	1,24705	1,32960	1,42686	1,54361
q=50 kN/ml ΔT=30°C P_{01}=0 kN	$\tau(x)$ (MPa)	4,00993	3,99569	3,98989	3,99635
	$\sigma_n(x)$ (MPa)	2,86432	2,86621	2,87591	2,89685
q=50 kN/ml ΔT=0°C P_{01}=20 kN	$\tau(x)$ (MPa)	-1,32072	-1,05967	-0,76800	-0,43759
	$\sigma_n(x)$ (MPa)	-0,85534	-0,66791	-0,45681	-0,21550
q=50 kN/ml ΔT=30°C P_{01}=20 kN	$\tau(x)$ (MPa)	0,99702	1,13837	1,30071	1,49026
	$\sigma_n(x)$ (MPa)	0,76194	0,86871	0,99224	1,13773
Case of the strengthened in support with Index of porosity μ = 0,02					
q=50 kN/ml ΔT=0°C P_{02}=0 kN	$\tau(x)$ (MPa)	0,45404	0,48302	0,51711	0,55799
	$\sigma_n(x)$ (MPa)	0,33454	0,35719	0,38397	0,41627
q=50 kN/ml ΔT=30°C P_{02}=0 kN	$\tau(x)$ (MPa)	2,77178	2,68106	2,58581	2,48584
	$\sigma_n(x)$ (MPa)	1,95183	1,89381	1,83302	1,76950
q=50 kN/ml ΔT=0°C P_{02}=10 kN	$\tau(x)$ (MPa)	-1,05242	-0,94564	-0,82748	-0,69506
	$\sigma_n(x)$ (MPa)	-0,71664	-0,64156	-0,55787	-0,46329
q=50 kN/ml ΔT=30°C P_{02}=10 kN	$\tau(x)$ (MPa)	1,26532	1,25240	1,24122	1,23280
	$\sigma_n(x)$ (MPa)	0,90064	0,89505	0,89118	0,88995

Fig. 12 Effect of the prestressing force of composite plate on interfacial stresses for a continuous RC damaged beam strengthened with presstresed composite plate

interfacial shear and normal stress for the RC damaged continuous beam strengthened with bonded prestressed FRP plate for the uniformly distributed load "q" case coupled with thermal load "ΔT", From these results, one can observe:

- Maximum stress occur at the ends of adhesively bonded plates, and the normal, or peeling, stress disappears at around 20 mm from the end of the plates.

- It is seen that increasing the value of prestressing force P_{01} and P_{02} leads to high stress concentrations.

4.3.5 Effect of porosity index of concrete "air bubble"

Following the analysis of the results obtained by varying the porosity of the concrete; while taking into account other parameters which influence the behavior of the beam reinforced by composite such as the variable of the damage and the coupled loading of the three loads namely: "q=50 kN/ml "the load uniformly distributed, P_0 the force of the prestressing (P_{01}=20 kN and P_{02}=10 kN) and the thermal load "ΔT=30°C". The peak of the stresses is recorded at the level of the porous concrete, that is to say that the more the concrete is porous the more becomes fragile and consequently a significant concentration of the stresses at the level of the interface.

As a recommendation, it is desirable to compact the concrete well during production in order to obtain a compact concrete which can withstand external stresses and to avoid all kinds of deterioration.

4. Conclusions

In this study, an improved adhesively bonded beam theory is proposed to model beam-type structures strengthened by an externally prestressed bonded plate. The ignored terms, such as the contribution of interface stresses on the deformations of adherends and the thermal effect coupled with the prestressed force in the existing solutions, have been included in the present model by introducing loading force. The improved solutions have been validated by comparing with the existing solutions. The effects of both the normal and shear deformations are presented and found to be an important factor influencing the interfacial stresses distribution in general. The present model provides more accurate prediction of the actual interfacial stresses distributions along the adhesively bonded interface. Furthermore, the improved solution is more generic in nature, and it is

Table 4 Effect of the prestressing force of composite plate on interfacial stresses for a continuous RC damaged beam strengthened with presstresed composite plate

Effect of the prestressing force of composite plate on interfacial stresses for a continuous RC damaged beam strengthened with presstresed composite plate							
Case of the strengthened in span with Index of porosity μ=0,02 and Damage variable φ=0,1							
Load	P_{01}	P_{01}=0 kN	P_{01}=10 kN	P_{01}=20 kN	P_{01}=30 kN	P_{01}=40 kN	P_{01}=50 kN
q=50 kN/ml	$\tau(x)$ (MPa)	1,79764	0,36898	-1,05968	-2,48834	-3,91700	-5,34566
ΔT=0°C	$\sigma_n(x)$ (MPa)	1,32960	0,33084	-0,66791	-1,66667	-2,66543	-3,66419
q=50 kN/ml	$\tau(x)$ (MPa)	3,99570	2,56704	1,13838	-0,29028	-1,71894	-3,14760
ΔT=30°C	$\sigma_n(x)$ (MPa)	2,86623	1,86747	0,86872	-0,13004	-1,12880	-2,12756
Case of the strengthened in support with Index of porosity μ=0,02 and Damage variable φ=0,1							
	P_{02}	P_{02}=0 kN	P_{02}=1 kN	P_{02}=2 kN	P_{02}=3 kN	P_{02}=4 kN	P_{02}=5 kN
q=50 kN/ml	$\tau(x)$ (MPa)	.483019	-.945641	-2.37430	-3.80296	-5.23162	-6.66028
ΔT=0°C	$\sigma_n(x)$ (MPa)	.357189	-.641568	-1.64032	-2.63908	-3.63784	-4.63659
q=50 kN/ml	$\tau(x)$ (MPa)	2.68106	1.25240	-.17626	-1.60492	-3.03358	-4.46224
ΔT=30°C	$\sigma_n(x)$ (MPa)	1.89381	.895053	-.10370	-1.10246	-2.10122	-3.09997

Table 5 Effect of porosity index of concrete on interfacial stresses for a continuous RC damaged beam strengthened with presstresed composite plate

Effect of porosity index of concrete on interfacial stresses for a continuous RC damaged beam strengthened with presstresed composite plate							
Case of the strengthened in span with Damage variable φ=0,1							
Load	Index of porosity	μ=0	μ=0,01	μ=0,02	μ=0,03	μ=0,04	μ=0,05
q=50 kN/ml ΔT=0°C P_{01}=0 kN	$\tau(x)$ (MPa)	1,77706	1,78727	1,79764	1,80816	1,81884	1,82967
	$\sigma_n(x)$ (MPa)	1,31345	1,32145	1,32959	1,33785	1,34624	1,35475
q=50 kN/ml ΔT=30°C P_{01}=0 kN	$\tau(x)$ (MPa)	3,99776	3,99669	3,99569	3,99475	3,99390	3,99311
	$\sigma_n(x)$ (MPa)	2,86535	2,86575	2,86620	2,86672	2,86732	2,86799
q=50 kN/ml ΔT=0°C P_{01}=20 kN	$\tau(x)$ (MPa)	-1,10972	-1,08482	-1,05967	-1,03426	-1,00860	-0,98266
	$\sigma_n(x)$ (MPa)	-0,70395	-0,68602	-0,66791	-0,64959	-0,63107	-0,61234
q=50 kN/ml ΔT=30°C P_{01}=20 kN	$\tau(x)$ (MPa)	1,11098	1,12459	1,13837	1,15232	1,16646	1,18078
	$\sigma_n(x)$ (MPa)	0,84796	0,85827	0,86871	0,87928	0,89001	0,90088
Case of the strengthened in support with Damage variable φ=0,1							
q=50 kN/ml ΔT=0°C P_{02}=0 kN	$\tau(x)$ (MPa)	0,47735	0,48016	0,48302	0,48591	0,48886	0,49184
	$\sigma_n(x)$ (MPa)	0,35275	0,35495	0,35719	0,35946	0,36176	0,36410
q=50 kN/ml ΔT=30°C P_{02}=0 kN	$\tau(x)$ (MPa)	2,69806	2,68957	2,68106	2,67250	2,66391	2,65527
	$\sigma_n(x)$ (MPa)	1,90466	1,89924	1,89381	1,88833	1,88284	1,87731
q=50 kN/ml ΔT=0°C P_{02}=10 kN	$\tau(x)$ (MPa)	-0,96604	-0,95589	-0,94564	-0,93530	-0,92486	-0,91433
	$\sigma_n(x)$ (MPa)	-0,65594	-0,64879	-0,64156	-0,63426	-0,62689	-0,61944
q=50 kN/ml ΔT=30°C P_{02}=10 kN	$\tau(x)$ (MPa)	1,25467	1,25352	1,25240	1,25129	1,25019	1,24910
	$\sigma_n(x)$ (MPa)	0,89597	0,89550	0,89505	0,89461	0,89419	0,89377

applicable to more general load cases and for the adherends made of all kinds of materials. The results obtained from the different analysis is agreed, which demonstrates that the present model is simple and accurate. Some studies of the taper are carried out in this work to better understand the effects of various parameters on the edge interfacial stresses in a structure under different applied load. In this work, our model takes into account the parameters neglected in the previous studies. This work is of paramount importance for designers of materials and structures to optimize their operation and life in the context of sustainable development.

Acknowledgments

References

Abdelouahed, T. (2006), "Improved theoretical solution for interfacial stresses in concrete beams strengthened with FRP plate", *Int. J. Solid. Struct.*, **43**(14-15), 4154-4174. https://doi.org/10.1016/j.ijsolstr.2005.03.074.
Abderezak, R., Daouadji, T.H. and Rabia, B. (2020), "Analysis of interfacial stresses of the reinforced concrete

foundation beams repairing with composite materials plate", *Coupl. Syst. Mech.*, **9**(5), 473-498. http://dx.doi.org/10.12989/csm.2020.9.5.473.

Abderezak, R., Daouadji, T.H. and Rabia, B. (2021), "Aluminum beam reinforced by externally bonded composite materials", *Adv. Mater. Res.*, **10**(1), 23. http://dx.doi.org/10.12989/amr.2021.10.1.023.

Abderezak, R., Daouadji, T.H. and Rabia, B. (2021), "Modeling and analysis of the imperfect FGM-damaged RC hybrid beams", *Adv. Comut. Des.*, **6**(2), 117. http://dx.doi.org/10.12989/acd.2021.6.2.117.

Abderezak, R., Daouadji, T.H., Abbes, B., Rabia, B., Belkacem, A. and Abbes, F. (2017), "Elastic analysis of interfacial stress concentrations in CFRP-RC hybrid beams: Effect of creep and shrinkage", *Adv. Mater. Res.*, **6**(3), 257. https://doi.org/10.12989/amr.2017.6.3.257.

Abderezak, R., Rabia, B., Daouadji, T.H., Abbes, B., Belkacem, A. and Abbes, F. (2018), "Elastic analysis of interfacial stresses in prestressed PFGM-RC hybrid beams", *Adv. Mater. Res.*, **7**(2), 83. https://doi.org/10.12989/amr.2018.7.2.083

Aicha, K., Rabia, B., Daouadji, T.H. and Bouzidene, A. (2020), "Effect of porosity distribution rate for bending analysis of imperfect FGM plates resting on Winkler-Pasternak foundations under various boundary conditions", *Coupl. Syst. Mech.*, **9**(6), 575. http://dx.doi.org/10.12989/csm.2020.9.6.575.

Akbaş, Ş.D. (2020), "Dynamic responses of laminated beams under a moving load in thermal environment", *Steel Compos. Struct.*, **35**(6), 729-737. http://dx.doi.org/10.12989/scs.2020.35.6.729.

Al-Furjan, M. S. H., Habibi, M., Ghabussi, A., Safarpour, H., Safarpour, M. and Tounsi, A. (2021), "Non-polynomial framework for stress and strain response of the FG-GPLRC disk using three-dimensional refined higher-order theory", *Eng. Struct.*, **228**, 111496. https://doi.org/10.1016/j.engstruct.2020.111496.

Al-Furjan, M.S.H., Habibi, M., Shan, L. and Tounsi, A. (2021), "On the vibrations of the imperfect sandwich higher-order disk with a lactic core using generalize differential quadrature method", *Compos. Struct.*, **257**, 113150. https://doi.org/10.1016/j.compstruct.2020.113150.

Al-Furjan, M.S.H., Safarpour, H., Habibi, M., Safarpour, M. and Tounsi, A. (2020), "A comprehensive computational approach for nonlinear thermal instability of the electrically FG-GPLRC disk based on GDQ method", *Eng. Comput.*, 1-18. https://doi.org/10.1007/s00366-020-01088-7.

Alimirzaei, S., Mohammadimehr, M. and Tounsi, A. (2019), "Nonlinear analysis of viscoelastic micro-composite beam with geometrical imperfection using FEM: MSGT electro-magneto-elastic bending, buckling and vibration solutions", *Struct. Eng. Mech.*, **71**(5), 485-502. http://dx.doi.org/10.12989/sem.2019.71.5.485.

Antar, K., Amara, K., Benyoucef, S., Bouazza, M. and Ellali, M. (2019), "Hygrothermal effects on the behavior of reinforced-concrete beams strengthened by bonded composite laminate plates", *Struct. Eng. Mech.*, **69**(3), 327-334. https://doi.org/10.12989/sem.2019.69.3.327.

Ashour, A.F., El-Refaie, S.A. and Garrity, S.W. (2004), "Flexural strengthening of RC continuous beams using CFRP laminates", *Cement Concrete Compos.*, **26**(7), 765-775. https://doi:10.1016/j.cemconcomp.2003.07.002

Benachour, A., Benyoucef, S. and Tounsi, A. (2008), "Interfacial stress analysis of steel beams reinforced with bonded prestressed FRP plate", *Eng. Struct.*, **30**(11), 3305-3315. https://doi.org/10.1016/j.engstruct.2008.05.007.

Bendada, A., Boutchicha, D., Khatir, S., Magagnini, E., Capozucca, R. and Wahab, M. A. (2020), "Mechanical characterization of an epoxy panel reinforced by date palm petiole particle", *Steel Compos. Struct.*, **35**(5), 627-634. http://doi.org/10.12989/scs.2020.35.5.627.

Benferhat, R., Daouadji, T.H. and Mansour, M.S. (2016), "Free vibration analysis of FG plates resting on an elastic foundation and based on the neutral surface concept using higher-order shear deformation theory", *Comptes Rendus Mecanique*, **344**(9), 631-641. https://doi.org/10.1016/j.crme.2016.03.002.

Benhenni, M.A., Daouadji, T.H., Abbes, B., Abbes, F., Li, Y. and Adim, B. (2019), "Numerical analysis for free vibration of hybrid laminated composite plates for different boundary conditions", *Struct. Eng. Mech.*, **70**(5), 535-549. https://doi.org/10.12989/sem.2019.70.5.535.

Benhenni, M.A., Daouadji, T.H., Abbes, B., Adim, B., Li, Y. and Abbes, F. (2018), "Dynamic analysis for anti-symmetric cross-ply and angle-ply laminates for simply supported thick hybrid rectangular plates", *Adv.*

Mater. Res., **7**(2), 119. https://doi.org/10.12989/amr.2018.7.2.119.

Bensattalah, T., Daouadji, T.H. and Zidour, M. (2019), "Influences the shape of the floor on the behavior of buildings under seismic effect", *International Symposium on Materials and Sustainable Development*, November. https://doi.org/10.1007/978-3-030-43268-3_3.

Bensattalah, T., Zidour, M. and Daouadji, T.H. (2018), "Analytical analysis for the forced vibration of CNT surrounding elastic medium including thermal effect using nonlocal Euler-Bernoulli theory", *Adv. Mater. Res.*, **7**(3), 163-174. https://doi.org/10.12989/amr.2018.7.3.163.

Chedad, A., Daouadji, T.H., Abderezak, R., Adim, B., Abbes, B., Rabia, B. and Abbes, F. (2017), "A high-order closed-form solution for interfacial stresses in externally sandwich FGM plated RC beams", *Adv. Mater. Res.*, **6**(4), 317-328. https://doi.org/10.12989/amr.2017.6.4.317.

Chergui, S., Daouadji, T.H., Hamrat, M., Boulekbache, B., Bougara, A., Abbes, B. and Amziane, S. (2019), "Interfacial stresses in damaged RC beams strengthened by externally bonded prestressed GFRP laminate plate: Analytical and numerical study", *Adv. Mater. Res.*, **8**(3), 197-217. https://doi.org/10.12989/amr.2019.8.3.197.

Chikr, S.C., Kaci, A., Bousahla, A.A., Bourada, F., Tounsi, A., Bedia, E.A., ... & Tounsi, A. (2020), "A novel four-unknown integral model for buckling response of FG sandwich plates resting on elastic foundations under various boundary conditions using Galerkin's approach", *Geomech. Eng.*, **21**(5), 471-487. http://dx.doi.org/10.12989/gae.2020.21.5.471.

Daouadji, H.T., Benyoucef, S., Tounsi, A., Benrahou, K.H. and Bedia, A.E. (2008), "Interfacial stress concentrations in FRP-damaged RC hybrid beams", *Compos. Interf.*, **15**(4), 425-440. https://doi.org/10.1163/156855408784514702.

Daouadji, T.H. (2013), "Analytical analysis of the interfacial stress in damaged reinforced concrete beams strengthened by bonded composite plates", *Strgth. Mater.*, **45**(5), 587-597. https://doi.org/10.1007/s11223-013-9496-4.

Daouadji, T.H. (2017), "Analytical and numerical modeling of interfacial stresses in beams bonded with a thin plate", *Adv. Comput. Des.*, **2**(1), 57-69. https://doi.org/10.12989/acd.2017.2.1.057.

Daouadji, T.H., Rabahi, A., Abbes, B. and Adim, B. (2016), "Theoretical and finite element studies of interfacial stresses in reinforced concrete beams strengthened by externally FRP laminates plate", *J. Adhes. Sci. Technol.*, **30**(12), 1253-1280. https://doi.org/10.1080/01694243.2016.1140703.

Daraei, B., Shojaee, S. and Hamzehei-Javaran, S. (2020), "Free vibration analysis of axially moving laminated beams with axial tension based on 1D refined theories using Carrera unified formulation", *Steel Compos. Struct.*, **37**(1), 37-49. http://dx.doi.org/10.12989/scs.2020.37.1.037

Guellil, M., Saidi, H., Bourada, F., Bousahla, A.A., Tounsi, A., Al-Zahrani, M.M., ... & Mahmoud, S.R. (2021), "Influences of porosity distributions and boundary conditions on mechanical bending response of functionally graded plates resting on Pasternak foundation", *Steel Compos. Struct.*, **38**(1), 1-15. http://dx.doi.org/10.12989/scs.2021.38.1.001.

Guenaneche, B. and Tounsi, A. (2014), "Effect of shear deformation on interfacial stress analysis in plated beams under arbitrary loading", *Int. J. Adhes. Adhesiv.*, **48**, 1-13. https://doi.org/10.1016/j.ijadhadh.2013.09.016.

Hadj, B., Rabia, B. and Daouadji, T.H. (2019), "Influence of the distribution shape of porosity on the bending FGM new plate model resting on elastic foundations", *Struct. Eng. Mech.*, **72**(1), 61-70. https://doi.org/10.12989/sem.2019.72.1.061.

Hadj, B., Rabia, B. and Daouadji, T.H. (2021), "Vibration analysis of porous FGM plate resting on elastic foundations: Effect of the distribution shape of porosity", *Coupl. Syst. Mech.*, **10**(1), 61-77. http://doi.org/10.12989/csm.2021.10.1.061.

Hamrat, M., Bouziadi, F., Boulekbache, B., Daouadji, T.H., Chergui, S., Labed, A. and Amziane, S. (2020), "Experimental and numerical investigation on the deflection behavior of pre-cracked and repaired reinforced concrete beams with fiber-reinforced polymer", *Constr. Build. Mater.*, **249**, 118745. http://doi.org/10.1016/j.conbuildmat.2020.118745.

Hassaine Daouadji, T., Bensattalah, T., Rabahi, A. and Tounsi, A. (2021), "New approach of composite wooden beam- reinforced concrete slab strengthened by external bonding of prestressed composite plate:

Analysis and modeling", *Struct. Eng. Mech.*, **78**(3), 319-332. http://dx.doi.org/10.12989/sem.2021.78.3.31.

He, X.J., Zhou, C.Y. and Wang, Y. (2019), "Interfacial stresses in reinforced concrete cantilever members strengthened with fibre-reinforced polymer laminates", *Adv. Struct. Eng.*, 1-12. https://doi.org/10.1177/1369433219868933.

Khatir, S., Tiachacht, S., Thanh, C.L., Bui, T.Q. and Wahab, M.A. (2019), "Damage assessment in composite laminates using ANN-PSO-IGA and Cornwell indicator", *Compos. Struct.*, **230,** 111509. https://doi.org/10.1016/j.compstruct.2019.111509.

Larrinaga, P., Garmendia, L., Piñero, I. and San-José, J.T. (2020), "Flexural strengthening of low-grade reinforced concrete beams with compatible composite material: Steel Reinforced Grout (SRG)", *Constr. Build. Mater.*, **235**, 117790. https://doi.org/10.1016/j.conbuildmat.2019.117790.

Liu, S., Zhou, Y., Zheng, Q., Zhou, J., Jin, F. and Fan, H. (2019), "Blast responses of concrete beams reinforced with steel-GFRP composite bars", *Struct.*, **22**, 200-212. https://doi.org/10.1016/j.istruc.2019.08.010.

Mansouri, L., Djebbar, A., Khatir, S. and Wahab, M.A. (2019), "Effect of hygrothermal aging in distilled and saline water on the mechanical behaviour of mixed short fibre/woven composites", *Compos. Struct.*, **207**, 816-825. https://doi.org/10.1016/j.compstruct.2018.09.067.

Mercan, K., Ebrahimi, F. and Civalek, O. (2020), "Vibration of angle-ply laminated composite circular and annular plates", *Steel Compos. Struct.*, 34(1), 141-154. http://doi.org/10.12989/scs.2020.34.1.141.

Panjehpour, M., Farzadnia, N., Demirboga, R. and Ali, A.A.A. (2016), "Behavior of high-strength concrete cylinders repaired with CFRP sheets", *J. Civil Eng. Manage.*, **22**(1), 56-64. https://doi.org/10.3846/13923730.2014.897965.

Rabahi, A., Daouadji, T.H., Abbes, B. and Adim, B. (2016), "Analytical and numerical solution of the interfacial stress in reinforced-concrete beams reinforced with bonded prestressed composite plate", *J. Reinf. Plast. Compos.*, **35**(3), 258-272. https://doi.org/10.1177/0731684415613633.

Rabia, B., Abderezak, R., Daouadji, T.H., Abbes, B., Belkacem, A. and Abbes, F. (2018), "Analytical analysis of the interfacial shear stress in RC beams strengthened with prestressed exponentially-varying properties plate", *Adv. Mater. Res.*, **7**(1), 29. https://doi.org/10.12989/amr.2018.7.1.029.

Rabia, B., Daouadji, T.H. and Abderezak, R. (2019), "Effect of distribution shape of the porosity on the interfacial stresses of the FGM beam strengthened with FRP plate", *Earthq. Struct.*, **16**(5), 601-609. https://doi.org/10.12989/eas.2019.16.5.601.

Rabia, B., Daouadji, T.H. and Abderezak, R. (2019), "Effect of porosity in interfacial stress analysis of perfect FGM beams reinforced with a porous functionally graded materials plate", *Struct. Eng. Mech.*, **72**(3), 293-304. https://doi.org/10.12989/sem.2019.72.3.293.

Rabia, B., Daouadji, T.H. and Abderezak, R. (2020), "Predictions of the maximum plate end stresses of imperfect FRP strengthened RC beams: study and analysis", *Adv. Mater. Res.*, **9**(4), 265. http://dx.doi.org/10.12989/amr.2020.9.4.265.

Rabia, B., Tahar, H.D. and Abderezak, R. (2020), "Thermo-mechanical behavior of porous FG plate resting on the Winkler-Pasternak foundation", *Coupl. Syst. Mech.*, **9**(6), 499-519. http://dx.doi.org/10.12989/csm.2020.9.6.499.

Rabia, B., Tahar, H.D. and Abderezak, R. (2021a), "Effect of porosity on fundamental frequencies of FGM sandwich plates", *Compos. Mater. Eng.*, **3**(1), 25-40. http://doi.org/10.12989/cme.2021.3.1.025.

Rabia, B., Tahar, H.D. and Abderezak, R. (2021b), "Effect of air bubbles in concrete on the mechanical behavior of RC beams strengthened in flexion by externally bonded FRP plates under uniformly distributed loading", *Compos. Mater. Eng.*, **3**(1), 41-55. http://doi.org/10.12989/cme.2021.3.1.041.

Sakr, M.A., Khalifa, T.M. and Mansour, W.N. (2016), "Analysis of RC continuous beams strengthened with FRP plates: A finite element model", *Civil Eng. J.*, **2**(11), 576-589. https://doi.org/10.28991/cej-2016-00000060.

Smith, S.T. and Teng, J.G. (2001), "Interfacial stresses in plated beams", *Eng. Struct.*, **23**(7), 857-871. http://dx.doi.org/10.1016/S0141-0296(00)00090-0.

Tahar, H.D., Abderezak, R. and Rabia, B. (2020), "Flexural performance of wooden beams strengthened by composite plate", *Struct. Monit. Mainten.*, **7**(3), 233-259. http://doi.org/10.12989/smm.2020.7.3.233.

Tahar, H.D., Boussad, A., Abderezak, R., Rabia, B., Fazilay, A. and Belkacem, A. (2019), "Flexural behaviour

of steel beams reinforced by carbon fibre reinforced polymer: Experimental and numerical study", *Struct. Eng. Mech.*, **72**(4), 409-420. https://doi.org/10.12989/sem.2019.72.4.409.

Tayeb, B. and Daouadji, T.H. (2020), "Improved analytical solution for slip and interfacial stress in composite steel-concrete beam bonded with an adhesive", *Adv. Mater. Res.*, **9**(2), 133-153. https://doi.org/10.12989/amr.2020.9.2.133.

Tlidji, Y., Benferhat, R. and Tahar, H.D. (2021), "Study and analysis of the free vibration for FGM microbeam containing various distribution shape of porosity", *Struct. Eng. Mech.*, **77**(2), 217. http://doi.org/10.12989/sem.2021.77.2.217.

Wang, Y.H., Yu, J., Liu, J.P., Zhou, B.X. and Chen, Y.F. (2020), "Experimental study on assembled monolithic steel-prestressed concrete composite beam in negative moment", *J. Constr. Steel Res.*, **167**, 105667. https://doi.org/10.1016/j.jcsr.2019.06.004.

Yuan, C., Chen, W., Pham, T.M. and Hao, H. (2019), "Effect of aggregate size on bond behaviour between basalt fibre reinforced polymer sheets and concrete", *Compos. Part B: Eng.*, **158**, 459-474. https://doi.org/10.1016/j.compositesb.2018.09.089.

Zenzen, R., Khatir, S., Belaidi, I., Le Thanh, C. and Wahab, M.A. (2020), "A modified transmissibility indicator and Artificial Neural Network for damage identification and quantification in laminated composite structures", *Compos. Struct.*, **248**, 112497. https://doi.org/10.1016/j.compstruct.2020.112497.

Zohra, A., Benferhat, R., Tahar, H.D. and Tounsi, A. (2021), "Analysis on the buckling of imperfect functionally graded sandwich plates using new modified power-law formulations", *Struct. Eng. Mech.*, **77**(6), 797-807. http://doi.org/10.12989/sem.2021.77.6.797.

DC